Online Appendix

Title: Dynamic Irrigation Management under Weather Uncertainty and Soil Heterogeneity

Erkut Sönmez, Barış Ata, Derek Heeren

A Proofs and Auxiliary Technical Results

This Appendix includes various technical results used to prove our main results stated in the main text as well as all proofs.

Lemma 1 *Under any irrigation policy with $u_t \geq 0$ for $t = 0, 1, \ldots, T-1$, we have that $x_{1,t} \geq x_t \geq x_{2,t} > 0$ for $t = 0, 1, \ldots, T$.*

Recall that x_t denotes the state trajectory under the original $A_t(\cdot)$ function that models the actual ET, whereas $x_{i,t}$ denotes the resulting state trajectory when $A_t(\cdot)$ is approximated by $A_{i,t}(\cdot)$ in Equation (2) for $i = 1, 2$.

Proof of Lemma 1. We proceed by induction. Note that $x_{1,0} = x_{2,0} = x_0 > 0$. Assume that the result holds for periods $\tau = 0, 1, \ldots, t$ and consider period $\tau = t + 1$. To that end, note that,

$$\xi_{2,t}(y) = A_{2,t}(y) - r_{2,t}(y) = P_t s_2 y - r_{2,t}(y).$$

Thus, we have the following:

$$x_{2,t+1} = x_{2,t} + u_t - \xi_{2,t}(x_{2,t} + u_t) = (1 - \frac{P_t}{S^c})(x_{2,t} + u_t) + r_{2,t}(x_{2,t} + u_t) > 0.$$

Note from Equation (2) and the definition of $r_t(y)$ that

$$x_{t+1} = \max\{x_t + u_t - A_t(x_t + u_t) + R_t, B\}. \tag{16}$$

Similarly, for $i = 1, 2$, we write

$$x_{i,t+1} = \max\{x_{i,t} + u_t - A_{i,t}(x_{i,t} + u_t) + R_t, B\}. \tag{17}$$

Also, we have from induction hypothesis that

$$x_{1,t} \geq x_t \geq x_{2,t} > 0. \tag{18}$$

In addition, the definition of $A_{i,t}(\cdot)$ for $i = 1, 2$ gives

$$A_{2,t} \geq A_t \geq A_{1,t}, \quad y \geq 0. \tag{19}$$

Lastly, we note that the following three quantities are increasing on $[0, B]$:

$$(i)\ \ y - A_t(y), \quad (ii)\ \ y - A_{1,t}(y), \quad (iii)\ \ y - A_{2,t}(y), \tag{20}$$

which follows from differentiating them by the virtue of Assumption 1. Combining these we write the following:

$$\begin{aligned}
x_{1,t+1} &= \max\{x_{1,t} + u_t - A_{1,t}(x_{1,t} + u_t) + R_t, B\} \\
&\geq \max\{x_t + u_t - A_{1,t}(x_t + u_t) + R_t, B\} \\
&\geq \max\{x_t + u_t - A_t(x_t + u_t) + R_t, B\} \\
&= x_{t+1} \\
&\geq \max\{x_{2,t} + u_t - A_t(x_{2,t} + u_t) + R_t, B\} \\
&\geq \max\{x_{2,t} + u_t - A_{2,t}(x_{2,t} + u_t) + R_t, B\} \\
&= x_{2,t+1},
\end{aligned}$$

where the first and third inequalities follow from the monotonicity of the expressions in Equation (20) and from Equation (18). The second and fourth inequalities follow from Equation (19), and the equalities follow from Equations (16) and (17). ■

Proof of Proposition 1. First, we let $\tilde{\mathcal{U}}$ denote the class of all irrigation policies with $u_t \geq 0$ for all t. Then we observe that $v_0(x) = \inf_{\vec{u} \in \mathcal{U}} J_0(x, \vec{u}) = \inf_{\vec{u} \in \tilde{\mathcal{U}}} J_0(x, \vec{u})$, because the restriction of $u_t \geq B - x_t$ we impose is without loss of optimality. Similarly, we note that $v_{i,0}(x) = \inf_{\vec{u} \in \tilde{\mathcal{U}}} J_{i,0}(x, \vec{u}),\ i = 1, 2$ and $x > 0$, where $J_{i,0}(x, \vec{u}) = \mathbb{E}\left\{\sum_{t=0}^{T-1} [c(u_t) + f_t(x_{i,t} + u_t)] + f_T(x_{i,T})\right\}$. Given an irrigation

policy $\vec{u} \in \tilde{\mathcal{U}}$, we deduce from Lemma 1 that $J_{1,0}(x, \vec{u}) \leq J_0(x, \vec{u}) \leq J_{2,0}(x, \vec{u})$. This follows because f_t is decreasing. Taking the infimum of all three over $\vec{u} \in \tilde{\mathcal{U}}$ yields the result. ■

As a preliminary to proving Theorem 1, we next establish several auxiliary results. First, we prove useful properties of the auxiliary function $\xi_{i,t}(\cdot)$ for $i = 1, 2$.

Lemma 2 *The functions $y - \xi_t(y)$ and $y - \xi_{i,t}(y)$ for $i = 1, 2$ are Lipschitz continuous on $[0, B]$ for $t = 0, 1, \ldots, T-1$.*

Proof of Lemma 2. Let $\mathbb{L} = 2(1 + \beta)$. Then it is straightforward to argue from Equation (3) that $|y - \xi(y) - (x - \xi(x))| \leq \mathbb{L}|y - x|$. The result for functions $y - \xi_{i,t}(y)$ for $i = 1, 2$ follows similarly. ■

Lemma 3 *For $i = 1, 2$ and $t = 0, 1, \ldots, T-1$, the function $y - \xi_{i,t}(y)$ is increasing and concave in y. Moreover, it is strictly increasing when $y - \xi_{i,t}(y) < B$.*

Proof of Lemma 3. Recall that $\xi_{i,t}(y) = P_t s_i y - r_{i,t}(y)$ for $i = 1, 2$. Substituting $r_{i,t}(y) = \min(R_t, B - y + P_t s_i y)$ yields the following:

$$y - \xi_{i,t}(y) = \min(y(1 - P_t s_i) + R_t, B),$$

from which the result follows. ■

The following lemma generalizes part (iii) of Proposition 4.1 of Sethi and Cheng (1997) so that it is applicable to our setting.

Lemma 4 *Letting ϕ be a decreasing and K-convex function, define the auxiliary function $\Phi_{i,t}(x) = \mathbb{E}[\phi(x - \xi_{i,t}(x))]$ for $i = 1, 2$, $t = 0, 1, \ldots, T-1$, and $x \in [0, B]$. Then $\Phi_{i,t}(x)$ is decreasing and K-convex for $i = 1, 2$, and $t = 0, 1, \ldots, T-1$.*

Proof of Lemma 4. Fix $t \geq 0$ and let $x_2 > x_1$, then $\phi(x_2 - \xi_{i,t}(x_2) \leq \phi(x_1 - \xi_{i,t}(x_1))$ for $i = 1, 2$, because $x_2 - \xi_{i,t}(x_2) \geq x_1 - \xi_{i,t}(x_1)$ by Lemma 3 and that ϕ is decreasing. Taking expectations, we conclude that

$$\Phi_{i,t}(x_2) = \mathbb{E}[\phi(x_2 - \xi_{i,t}(x_2))] \leq \mathbb{E}[\phi(x_1 - \xi_{i,t}(x_1))] = \Phi_{i,t}(x_1), i = 1, 2.$$

That is, $\Phi_{i,t}$ is decreasing. Next, to establish its K-convexity, we check the following (see Porteus, 2002): For $y, x \in [0, B]$ with $y > x$ and $\lambda \in [0, 1]$,

$$\lambda\Phi_{i,t}(x) + (1-\lambda)[\Phi_{i,t}(y) + K_f] \geq \Phi_{i,t}(\lambda x + (1-\lambda)y). \tag{21}$$

This is equivalent to checking that

$$\lambda\mathbb{E}[\phi(x - \xi_{i,t}(x))] + (1-\lambda)[\mathbb{E}[\phi(y - \xi_{i,t}(y))] + K_f] \geq \mathbb{E}[\phi(\lambda x + (1-\lambda)y - \xi_{i,t}(\lambda x + (1-\lambda)y))]. \tag{22}$$

(Note that $y - \xi_{i,t}(y) \geq x - \xi_{i,t}(x)$ by Lemma 3 because $y > x$.) On the other hand, because g is K-convex, for $x_1 < x_2$ and $\lambda \in [0, 1]$, we have that

$$\lambda\phi(x_1) + (1-\lambda)[\phi(x_2) + K_f] \geq \phi(\lambda x_1 + (1-\lambda)x_2). \tag{23}$$

Because $x < y$ and $\lambda \in [0, 1]$, we note from concavity of $x - \xi_{i,t}(x)$ that

$$\lambda(x - \xi_{i,t}(x)) + (1-\lambda)(y - \xi_{i,t}(y)) \leq \lambda x + (1-\lambda)y - \xi_{i,t}(\lambda x + (1-\lambda)y). \tag{24}$$

Then, because ϕ is decreasing, we conclude that

$$\phi(\lambda(x - \xi_{i,t}(x)) + (1-\lambda)(y - \xi_{i,t}(y))) \geq \phi(\lambda x + (1-\lambda)y - \xi_{i,t}(\lambda x + (1-\lambda)y)). \tag{25}$$

Combining (23) and (25) (with $x_1 = x - \xi_{i,t}(x) < x_2 = y - \xi_{i,t}(y)$) gives

$$\begin{aligned}\lambda\phi(x - \xi_{i,t}(x)) + (1-\lambda)(\phi(y - \xi_{i,t}(y)) + K_f) &\geq \phi(\lambda(x - \xi_{i,t}(x)) + (1-\lambda)(y - \xi_{i,t}(y))) \\ &\geq \phi(\lambda x + (1-\lambda)y - \xi_{i,t}(\lambda x + (1-\lambda)y)).\end{aligned}$$

That is, $\lambda\phi(x - \xi_{i,t}(x)) + (1-\lambda)[\phi(y - \xi_{i,t}(y)) + K_f] \geq \phi(\lambda x + (1-\lambda)y - \xi_{i,t}(\lambda x + (1-\lambda)y))$. Taking the expectations of both sides gives (21), completing the proof. ■

Next, we prove certain structural properties of the value function $v_{i,t}$, which help us to prove Theorem 1.

Lemma 5 *For $i = 1, 2$ and $t = 0, 1, \ldots, T$, $v_{i,t}(\cdot)$ is nonnegative, decreasing and Lipschitz contin-*

uous.

Proof of Lemma 5. We proceed by induction. Recall that for $i = 1, 2$, $x \in [0, B]$, $v_{i,T}(x) = f_T(x)$. Thus, $v_{i,T}(\cdot)$ is nonnegative, decreasing and Lipschitz continuous (with Lipschitz constant L_T). Assume the result holds for $t+1, \ldots, T$ and consider $v_{i,t}(\cdot)$. Recall that

$$v_{i,t}(x) = \inf_{u \in [0, B-x]} \{c(u) + f_t(x+u) + \mathbb{E}\left[v_{i,t+1}(x + u - \xi_{i,t}(x+u))\right]\} \tag{26}$$

First, we establish that $v_{i,t}(\cdot)$ is nonnegative. Note that $f_t(\cdot)$, $c(\cdot)$, and $v_{i,t+1}(\cdot)$ are all nonnegative. Thus, so is the right-hand side of (26). That is, $v_{i,t}(\cdot)$ is nonnegative. Second, we establish that $v_{i,t}(\cdot)$ is decreasing. To this end, let $x_2 > x_1$ with $x_1, x_2 \in [0, B]$. By virtue of Equation (26), for $\epsilon > 0$, there exists $\tilde{u}_1 \in [0, B - x_1]$ such that

$$c(\tilde{u}_1) + f_t(x_1 + \tilde{u}_1) + \mathbb{E}[v_{i,t+1}(x_1 + \tilde{u}_1 - \xi_{i,t}(x_1 + \tilde{u}_1))] \leq v_{i,t}(x_1) + \epsilon. \tag{27}$$

We have two cases to consider: Case (i) $x_2 < x_1 + \tilde{u}_1$, and case (ii) $x_2 \geq x_1 + \tilde{u}_1$.
Case (i) $x_2 < x_1 + \tilde{u}_1$: In this case let $\tilde{u}_2 = x_1 + \tilde{u}_1 - x_2 < \tilde{u}_1$ and note that

$$\begin{aligned} v_{i,t}(x_2) &\leq c(\tilde{u}_2) + f_t(x_2 + \tilde{u}_2) + \mathbb{E}[v_{i,t+1}(x_2 + \tilde{u}_2 - \xi_{i,t}(x_2 + \tilde{u}_2))] \\ &= c(\tilde{u}_2) + f_t(x_1 + \tilde{u}_1) + \mathbb{E}[v_{i,t+1}(x_1 + \tilde{u}_1 - \xi_{i,t}(x_1 + \tilde{u}_1))] \\ &\leq c(\tilde{u}_1) + f_t(x_1 + \tilde{u}_1) + \mathbb{E}[v_{i,t+1}(x_1 + \tilde{u}_1 - \xi_{i,t}(x_1 + \tilde{u}_1))] \\ &\leq v_{i,t}(x_1) + \epsilon, \end{aligned} \tag{28}$$

where the first inequality follows from the definition of $v_{i,t}$ (see Equation (26)), whereas the equality follows because $x_2 + \tilde{u}_2 = x_1 + \tilde{u}_1$. The second inequality follows because $c(\tilde{u}_1) > c(\tilde{u}_2)$. The last inequality follows from Equation (27).

Case (ii) $x_2 \geq x_1 + \tilde{u}_1$: In this case, note that

$$\begin{aligned} v_{i,t}(x_2) &\leq 0 + f_t(x_2) + \mathbb{E}[v_{i,t+1}(x_2 - \xi_{i,t}(x_2))] \\ &\leq c(\tilde{u}_1) + f_t(x_1 + \tilde{u}_1) + \mathbb{E}[v_{i,t+1}(x_1 + \tilde{u}_1 - \xi_{i,t}(x_1 + \tilde{u}_1))] \\ &\leq v_{i,t}(x_1) + \epsilon, \end{aligned} \tag{29}$$

where the first inequality follows from Equation (26) by setting $u_t = 0$, which is feasible but not necessarily optimal. The second inequality follows because $f_t(x_2) < f_t(x_1 + \tilde{u}_1)$, $0 \leq c(\tilde{u}_1)$, and that $v_{i,t+1}$ is decreasing by induction hypothesis and $x_2 - \xi_{i,t}(x_2) \geq x_1 + \tilde{u}_1 - \xi_{i,t}(x_1 + \tilde{u}_1)$, which in turn follows because $x_1 + \tilde{u}_1 \leq x_2$ and $y - \xi_{i,t}(y)$ is increasing by Lemma 4. The last inequality follows from Equation (27).

Combining Equations (28) - (29) gives $v_{i,t}(x_2) \leq v_{i,t}(x_1) + \epsilon$. Then letting $\epsilon \downarrow 0$ shows $v_{i,t}(\cdot)$ is decreasing.

Lastly, we show that $v_{i,t}$ is Lipschitz continuous. By the induction hypothesis, we have that

$$|v_{i,t+1}(x) - v_{i,t+1}(y)| \leq L_{t+1}|x - y|.$$

We wish to prove that for some $L_t > 0$,

$$-L_t|x - y| \leq |v_{i,t}(x) - v_{i,t}(y)| \leq L_t|x - y|. \tag{30}$$

Without loss of generality, we assume $y > x$. We already know by the preceding analysis that $v_{i,t}(y) \leq v_{i,t}(x)$, i.e. $v_{i,t}(x) - v_{i,t}(y) \geq 0$. Thus, the first inequality in (30) is readily satisfied and we only need to show that $v_{i,t}(x) < v_{i,t}(y) + L_t|y - x|$. Let $\tilde{u}_2$ be such that (cf. Equation (26))

$$v_{i,t}(y) \geq c(\tilde{u}_2) + f_t(y + \tilde{u}_2) + \mathbb{E}[v_{i,t+1}(y + \tilde{u}_2 - \xi_{i,t}(y + \tilde{u}_2))] - \epsilon. \tag{31}$$

We also note from Equation (26) that

$$v_{i,t}(x) \leq c(\tilde{u}_2) + f_t(x + \tilde{u}_2) + \mathbb{E}[v_{i,t+1}(x + \tilde{u}_2 - \xi_{i,t}(x + \tilde{u}_2))]. \tag{32}$$

(Note that $\tilde{u}_2$ is feasible at state x, i.e. $0 \leq \tilde{u}_2 \leq B - x$, because $x < y$ and $\tilde{u}_2$ is feasible for state y.) Using (32) and the facts that f_t, $v_{i,t+1}$ and $(x - \xi_{i,t}(x))$ are Lipschitz continous, we write

$$v_{i,t}(x) \leq c(\tilde{u}_2) + f_t(y + \tilde{u}_2) + c_1|y - x| + c_2|y - x| + \mathbb{E}[v_{i,t+1}(y + \tilde{u}_2 - \xi_{i,t}(y + \tilde{u}_2))] \tag{33}$$

where $c_1, c_2 > 0$ are suitably defined constants. Combining (31) and (33) gives $v_{i,t}(x) \leq (c_1 + c_2)|y - x| + v_{i,t}(y) + \epsilon$. Letting $L_t = c_1 + c_2$ and $\epsilon \downarrow 0$, we conclude that $v_{i,t}(x) - v_{i,t}(y) \leq L_t|y - x|$, completing the proof. ■

Proof of Theorem 1. Fix $i \in \{1, 2\}$ and note that the dynamic programming equations can be written as follows:

$$v_{i,t}(x) = -cx + h_{i,t}(x), \ t = 0, 1, \ldots, T - 1, \tag{34}$$

$$v_{i,T}(x) = f_T(x), \tag{35}$$

where

$$h_{i,t}(x) = \inf_{y \in [x, B-x]} \left[K_f \mathbb{1}_{\{y > x\}} + z_{i,t}(y) \right], \text{ and} \tag{36}$$

$$z_{i,t}(y) = cy + f_t(y) + \mathbb{E}[v_{i,t+1}(y - \xi_{i,t}(y))]. \tag{37}$$

As an aside note that because $v_{i,t}$ is nonnegative, $z_{i,t}(y) \geq cy \geq cx$. Moreover, $z_{i,t}(\cdot)$ is Lipschitz continuous by Lemma 5. Next, we prove that $z_{i,t}$, $h_{i,t}$ and $v_{i,t}$ are K-convex. Because $v_{i,T}(x) = f_T(x)$, which is convex, it follows from Equation (37), Lemma 4 and the convexity of f_{T-1} that $z_{i,T-1}$ is K-convex. Then it follows from Proposition 4.2 (iii) of Sethi and Cheng (1997) that $h_{i,T-1}$ is K-convex, which in turn, implies $v_{i,T-1}$ is K-convex by virtue of Equation (34). This establishes the induction basis. Let us assume $z_{i,\tau}$, $h_{i,\tau}$, and $v_{i,\tau}$ are K-convex for $\tau = t + 1, \ldots, T - 1$. As argued immediately above, K-convexity of $v_{i,t+1}$, Lemma 4, and convexity of f_t yield K-convexity of $z_{i,t}$. Then Proposition 4.2 (iii) of Sethi and Cheng (1997) implies K-convexity of $h_{i,t}$. From this and Equation (34), the K-conveity of $v_{i,t}$ is immediate. Therefore, $z_{i,t}$, $h_{i,t}$, and $v_{i,t}$ are K-convex for $t = 1, \ldots, T - 1$. Combining this with Lemma 4, Bellman Equation (6) and the convexity of f_t, we conclude that a time-dependent (s, S) policy is optimal, see for example, Porteus (2002).

Moreover, Proposition 4.2 of Sethi and Cheng (1997) yields the desired parameters (s_t, S_t) for $t = 0, 1, \ldots, T-1$. ■

Next, we present an algorithm to compute the parameters of the optimal policy. To do so, for $i = 1, 2$ and $t = 0, 1, \ldots, T-1$ we define

$$z_{i,t}(y) = cy + f_t(y) + \mathbb{E}[v_{i,t+1}(y - \xi_{i,t}(y))], \quad y \in [0, B],$$
$$z^*_{i,t} = \inf \{z_{i,t}(y) : y \in [0, B]\}.$$

Fixing $i \in \{1, 2\}$, the following algorithm describes how to compute the parameters for the corresponding approximation.

Algorithm 1 *Computation of thresholds s_t and S_t*

1: Set $t = T - 1$.
2: Solve for $S_t = \arg\min \left\{ x \in [0, B] | z_{i,t}(x) = z^*_{i,t} \right\}$.
3: Solve for $s_t = \min \{x \in [0, S_t] | z_{i,t}(x) \leq K_f + z_{i,t}(S_t)\}$.
4: **if** $t > 0$, set $t = t - 1$ and go to Step 2, **otherwise** go to Step 5.
5: **end**.

The next two lemmas facilitate the proof of Proposition 2, where Lemma 6 compares the auxiliary process $y - \xi(y)$ across soil types under the two AET approximations. Similarly, Lemma 7 provides such a comparison under the original AET process.

Lemma 6 *For $t = 0, 1, \ldots, T-1$, and $l < j \in \{1, \ldots, L\}$, and $i = 1, 2$, we have that*

(i) $y - \xi^j_{i,t}(y) \geq y - \xi^l_{i,t}(y)$, $y \in [0, B^l]$,

(ii) $y - \xi^j_{i,t}(y) \geq B^l - \xi^l_{i,t}(B^l)$, $y \in [B^l, B^j]$.

Proof of Lemma 6. First, consider $i = 1$ and note that $y \in [0, B^l]$. We have

$$y - \xi^j_{1,t}(y) = \min \left\{ y(1 - \frac{P_t}{B^j}) + R_t, B^j \right\},$$
$$y - \xi^l_{1,t}(y) = \min \left\{ y(1 - \frac{P_t}{B^l}) + R_t, B^l \right\}.$$

Because $B^l < B^j$ and

$$\frac{P_t}{B^j} < \frac{P_t}{B^l} \leq \frac{P_t}{B^1} \leq \frac{P_t}{S^{1,c}} \leq \beta < 1 \quad \text{for all } t,$$

(i) follows; and (ii) follows because $y - \xi_{i,t}^j(y)$ is increasing on $[B^l, B^j]$. The case of $i = 2$ follows similarly. ■

Lemma 7 *For $t = 0, 1, \ldots, T-1$, and $l < j \in \{1, \ldots, L\}$, we have that*

(i) $y - \xi_t^j(y) \geq y - \xi_t^l(y)$, $y \in [0, B^l]$,

(ii) $y - \xi_t^j(y) \geq B^l - \xi_t^l(B^l)$, $y \in [B^l, B^j]$.

Proof of Lemma 7. Note that for $y \in [0, B^l]$, we have that

$$y - \xi_t^j(y) = \min\left\{y - P_t \min(\frac{y}{S^{j,c}}, 1) + R_t, B^j\right\},$$
$$y - \xi_t^l(y) = \min\left\{y - P_t \min(\frac{y}{S^{l,c}}, 1) + R_t, B^l\right\},$$

from which (i) follows. Moreover, (ii) follows from (i) at $y = B^l$, because $y - \xi_t^j(y)$ is increasing on $[B^l, B^j]$. ■

Proof of Proposition 2. By Assumption 2 $x_{i,t}^L \geq x_{i,t}^{L-1} \geq \ldots \geq x_{i,t}^1$ holds for $t = 0$. Assume it holds for $t = 1, \ldots, \tau$ and consider $t = \tau + 1$. Let $l < j$.

$$x_{i,\tau+1}^j = x_{i,\tau}^j + u_\tau - \xi_{i,\tau}^j(x_{i,\tau}^j + u_t) \geq x_{i,\tau}^j + u_\tau - \xi_{i,\tau}^l(x_{i,\tau}^j + u_t) \geq x_{i,\tau}^l + u_\tau - \xi_{i,\tau}^l(x_{i,\tau}^l + u_t),$$

where the first inequality follows from Lemma 6 and that $i < j$. The second inequality follows from Lemma 3. The proof of $x_t^L \geq x_t^{L-1} \geq \ldots \geq x_t^1$ proceeds similarly, but it uses Lemma 7 instead of Lemma 6.

We now turn to the proof of $x_{1,t}^l \geq x_t^l \geq x_{2,t}^l$ for all t, l. To prove this, we will use the following two facts (see Equations (19)-(20)):

$$A_{2,t}(y) \geq A_t(y) \geq A_{1,t}(y), \text{ for } y \geq 0, \tag{38}$$

$$y - A_t(y),\ y - A_{i,t}(y) \text{ for } i = 1, 2 \text{ are nondecreasing.} \tag{39}$$

Note that $x^l_{1,0} = x^l_0 = x^l_{2,0}$, constituting the induction basis. Assume $x^l_{1,t} \geq x^l_t \geq x^l_{2,t}$ for $t = 0, 1, \ldots, \tau$ and consider $t = \tau + 1$.

$$\begin{aligned}
x^l_{1,t+1} &= \max\{x^l_{1,t} + u_t - A_{1,t}(x^l_{1,t} + u_t) + R_t, B^l\} \\
&\geq \max\{x^l_t + u_t - A_{1,t}(x^l_t + u_t) + R_t, B^l\} \\
&\geq \max\{x^l_t + u_t - A_t(x^l_t + u_t) + R_t, B^l\} \\
&= x^l_{t+1} \\
&\geq \max\{x^l_{2,t} + u_t - A_t(x^l_{2,t} + u_t) + R_t, B^l\} \\
&\geq \max\{x^l_{2,t} + u_t - A_{2,t}(x^l_{2,t} + u_t) + R_t, B^l\} \\
&= x^l_{2,t+1},
\end{aligned}$$

where the first and third inequalities follow from Equation (39) and the inductive hypothesis. The second and fourth inequalities follow from Equation (38), and the equalities follow from state dynamics given a control. ■

Proof of Proposition 3. Let e denote the I-dimensional vector of ones, and note that $\tilde{f}_t(y_L) = F_t(y_L e)$ and $\tilde{f}_t(y_1) = F_t(y_1 e)$. By componentwise monotonicity of F_t and that $y^L \geq \ldots \geq y^1$, we note that $\tilde{f}_t(y_L) = F_t(y_L e) \leq F_t(\vec{y}) \leq F_t(y_1 e) = \tilde{f}_t(y_1)$. ■

Proof of Proposition 4. Recall that $\tilde{v}_{i,0}(\vec{x}) = \inf_{\vec{u}} \tilde{J}_{i,0}(\vec{x}, \vec{u})$ where $\tilde{J}_{i,t}$ is given by Equation (11). Similarly, $\tilde{v}_0(\vec{x}) = \inf_{\vec{u}} \tilde{J}_0(\vec{x}, \vec{u})$ where $\tilde{J}_t$ is given by Equation (10). Given control $\vec{u}$, because we have $x^l_{2,t} \leq x^l_t \leq x^l_{1,t}$ for all l, t by Proposition 2 and F_t is decreasing in each of its components, we conclude from Equations (10) - (11) that $\tilde{J}_{2,0}(\vec{x}, \vec{u}) \leq \tilde{J}_0(\vec{x}, \vec{u}) \leq \tilde{J}_{1,0}(\vec{x}, \vec{u})$, from which (i) follows.

Proof of (ii) (respectively (iii)) follows similarly, but it uses Equations (13) and (15) (respectively ((12) and (14)) along with the monotonicity of $\tilde{f}_t$ and that $x^L_{2,t} \leq x^L_t \leq x^L_{1,t}$ for all t (respectively, $x^1_{2,t} \leq x^1_t \leq x^1_{1,t}$ for all t) to conclude $\underline{J}_1(x^L, \vec{u}) \leq \underline{J}(x^L, \vec{u}) \leq \underline{J}_2(x^L, \vec{u})$ (respectively, $\bar{J}_1(x^1, \vec{u}) \leq \bar{J}(x^1, \vec{u}) \leq \bar{J}_2(x^1, \vec{u})$) from which (ii) (respectively (iii)) follows. ■

B Alfalfa Numerical Study

Our model of soil water, ET, and yield relation applies to a broad range of crop types because the crops follow the same soil water uptake and biomass production processes. On the other hand, some coefficients used in such approximate formulations can be crop specific and are determined by empirical field studies in the agriculture literature. One can refer to FAO's guidelines for crop specific coefficient values (for instance, Doorenbos and Kassam (1979) (FAO33), Allen et al. (1998) (FAO56), and Steduto et al. (2012) (FAO66)).

As we discussed in Section 3.1, potential ET (PET) reflects a crop's water demand to provide the maximum yield. In addition, a crop's water sensitivity is correlated with its PET. For annual crops, such as wheat, soybean, corn, potato, etc., both the PET and the water sensitivity are low during early and maturity stages, and they are higher during the middle development and reproductive periods (Allen et al. 1998; Eisenhauer et al. 2021). Thus, different annual crops have similar bell-shaped distributions for their PET and sensitivity as presented in Figure 5. Thus, our modeling framework and numerical insights presented in Section 3.1 (based on corn data) will be valid for other annual crops as well.

We repeat our analysis focusing on growing alfalfa in California to extend our numerical study with different crop and location characteristics. Alfalfa is the oldest and most important forage crop globally which is grown over 70 countries worldwide. It can be used for grazing (for dairy cows, chickens, sheep, pigs, etc.) or used as hay, silage, green manure and as a cover crop. Alfalfa is also edible (for human consumption); it contains high levels of essential vitamins and minerals. We select alfalfa as its PET and water sensitivity (such as presented in Figures 6 and 9) do not follow a bell shape pattern. This is due to its distinct growth characteristics associated with its

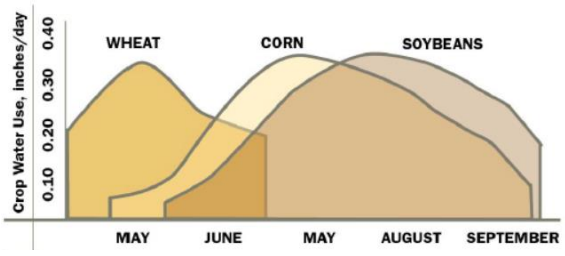

Figure 5: Example of daily ET patterns for wheat, corn, and soybeans (Source: Bauder et al., 2009).

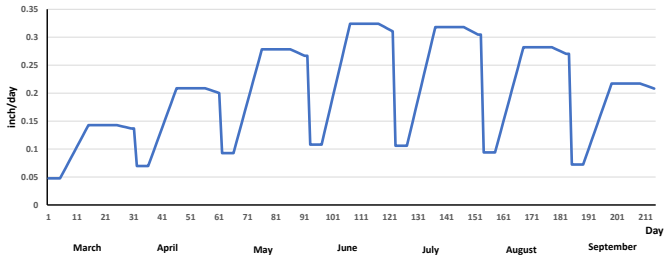

Figure 6: Average daily PET with harvest schedule of every 30 days.

perennial nature. (Perennial plants, unlike like annual crops, live multiple years without the need for replanting each year. Many fruit and nut trees along with grapes, cotton, sugar cane, asparagus, and artichoke are other examples of perennial plants.) Alfalfa is harvested (cut) multiple times throughout a growing season. In California, alfalfa growing season is between March and October with an average cut of every 30 days (Doorenbos and Kassam 1979; Allen et al. 1998; Putnam et al. 2007). After each cut, it grows back quickly, thus, it is initial growth period is much shorter compared to annual crops. In addition, PET in its late period decreases slightly, as opposed to significant decrease in annual crops, due to its slower self-shading and senescence. These growth characteristics result in its distinct PET and water sensitivity patterns compared to the annual crops.

In addition, California receives limited rainfall. For example, historical rainfall in Parlier, California and irrigation need for alfalfa farming are presented in Figures 7 and 8, respectively. California has been among the top alfalfa producing states and alfalfa has been among state's highest acreage crops as California is the leading diary producer (Putnam et al. 2007). Alfalfa consumes the most irrigation water in California and covers the 9% of the total irrigated acres (more than any other crop)(USDA 2019; Putnam et al. 2007). Alfalfa is produced throughout California with the major production zone of San Joaquin Valley (61% of the state's production) (Putnam et al. 2007).

We select Parlier, California as the location of our field. Parlier is in Fresno County located at the San Joaquin Valley, which is one of the main alfalfa growing regions in California. We obtain climate data from California Irrigation Management Information System's (CIMIS) Parlier weather station (https://cimis.water.ca.gov/, accessed on 11/10/2022). This dataset includes daily

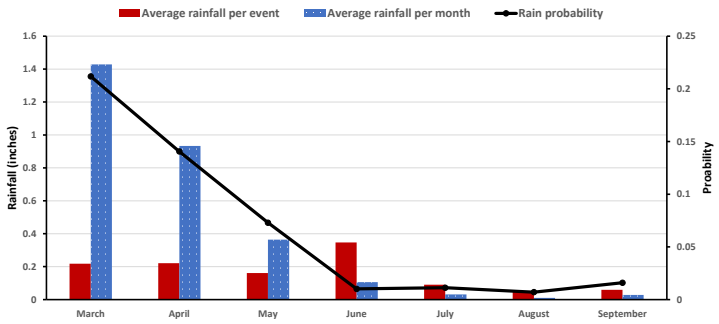

Figure 7: Rainfall pattern in Parlier, CA.

PET and precipitation measurement between 2000 and 2022. Figure 6 presents average daily PET as a function of time during the growing season. It decreases right after the harvest and then rapidly reaches to maximum where it will stay until the next harvest. One can refer to Allen et al. (1998) Tables 11 and 12 for alfalfa growth stages and durations in California. We estimate the daily PET during the growing season using Parlier weather station data. We present the histograms of daily PET values for a sample of months in Appendix C. For each month, we fit a discrete probability distribution to the daily PET values using our climate dataset.

Similarly, using our dataset, we characterize the rainfall pattern in Parlier, CA during the growing season. See Figure 7 for the daily rain probability and the average rainfall per month and per rain event. We fit a discrete probability distribution to rainfall per rainy day (that is, conditional on the rain event) using our climate dataset, see Appendix C for the histograms of daily rainfall.

Following our PET and rainfall analysis, Figure 8 presents the average monthly PET and rainfall

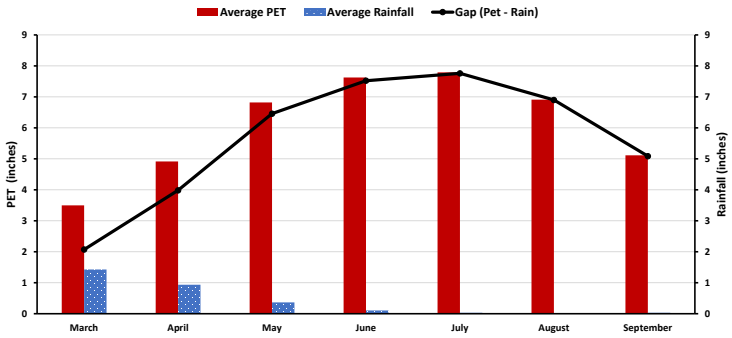

Figure 8: Monthly PET and rainfall in Parlier, CA.

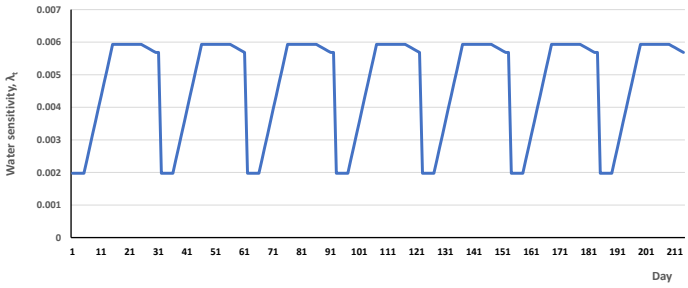

Figure 9: Daily yield water sensitivity index for alfalfa, λ_t.

amounts along with the gap between these two quantities (gap is PET minus rainfall). This figure reveals that alfalfa heavily depends on irrigation to achieve maximum yield especially during the second half of the growing where there is hardly any rainfall.

We also present the water sensitivity index throughout the growing season in Figure 9. For each harvest cycle, we estimate lambda with the ratio of the average PET of a given period to the average cumulative PET throughout the harvest cycle, as done in Section 3.1.

Following Hansen et al. (2008), we assume the soil type in our field to be silt loam with an effective root depth of 5 feet. For silt-loam soil, upper and lower limits (field capacity and wilting point) are 18 inches and 9 inches, respectively, for 5 feet root depth (Enciso et al. 2012, Table 1). In addition, water stress starts at about 50% of the soil water storage capacity (Enciso et al. 2012, Table 2). Following these soil characteristics, we set our normalized soil parameters as $B = 9$, $w = 0$, and $S^c = 4.5$ inches.

Several articles discuss drying wells and increasing well depths in California following extended droughts in recent years and increasing irrigation, domestic, and public freshwater demand (Chea 2022; La Ganga et al. 2021; Becker 2021; Cagle 2020; Stockstad 2020; Jasechko and Perrone 2020). To analyze well depth, we use well completion reports dataset from California Department of Water Resources (available at https://data.cnra.ca.gov/dataset/well-completion-reports, accessed on 01/10/2023). In our analysis, we focus on irrigation wells reports received within the last 5 years (2018 - 2022) in Fresno County following the increasing well depths in recent years. This dataset contains 908 well reports with a median well depth of 122 meters and with 92 and 161 meters at the 25th and 75th percentiles, respectively.

We set the maximum attainable yield as $Y_{max} = 8.9$ tons/acre (22 tons/hectare) based on a

growing season (March to October) involving 7 cuts (Doorenbos and Kassam 1979). For alfalfa and diesel prices, we use the average price in California for the last 5 year (2018 -2022), that are, \$218.3/ton and \$4.27/gallon, respectively (retrieved from https://usda.library.cornell.edu/concern/publications/c821gj76b and www.eia.gov/petroleum/, accessed on 01/15/2023). Following the parameters given above and formulation presented by Eisenhauer et al. (2021) (chapter 8.7), we calculate the variable and fixed irrigation costs for the median well depth of 122 meters as \$23.17 per inch per acre and \$4.63 per acre.

First, we study the case where we use the median well depth of 122 meters. In practice, extension services suggest the FC policy (discussed in Section 3.1.2) to farmers for alfalfa irrigation in California (Hansen et al. 2008). Recall that, in the FC policy, the farmer irrigates up to the upper limit whenever the water level decreases to S^c. Similar to Section 3.1.2, we also study the best fixed irrigation amount for the stress-avoidance policies. We find that for each well-depth we study, the FC policy provides the highest net return among the fixed irrigation amounts to be used in every irrigation event. Thus, in our analysis, we compare the proposed (s, S)-type 1 and (s, S)-type 2 policies with the FC policy. However, we also include a 2-inch fixed irrigation policy (where the farmer irrigates 2 inches of water whenever it decreases to S^c) in our comparison to provide insights on additional policies applicable in practice. As in Section 3.1.2, to compare different irrigation policies, we use our simulation model that mimics the original soil water hydrologic cycle discussed in Section 3. Specifically, in our simulation model, we use the original actual ET function, $A_t(\cdot)$, rather than the approximations we used for (s, S)-type 1 and (s, S)-type 2 policies, $A_{i,t}(\cdot)$, $i = 1, 2$ (see Figure 1). For each irrigation policy, we replicate our simulation 1000 times. The half-width of a 95% confidence interval of the estimate of each performance metric calculated is less than 0.5% of the mean. We calculate optimal (s, S) thresholds for the proposed irrigation policy using Mathematica software.

Figure 10 presents the (s, S) thresholds for the type 1 and 2 irrigation policies. For both policies, (s, S) thresholds follow stable patterns throughout the growing season. This is due to alfalfa's short initial and late growth stages (compared to development and middle stages) and the repeating harvest cycles, as presented in Figures 6 and 9.

Tables 5 and 6 compare the irrigation policies in terms of normalized net return (revenue minus irrigation cost), yield, and water usage. All metrics are provided per acre of land. These perfor-

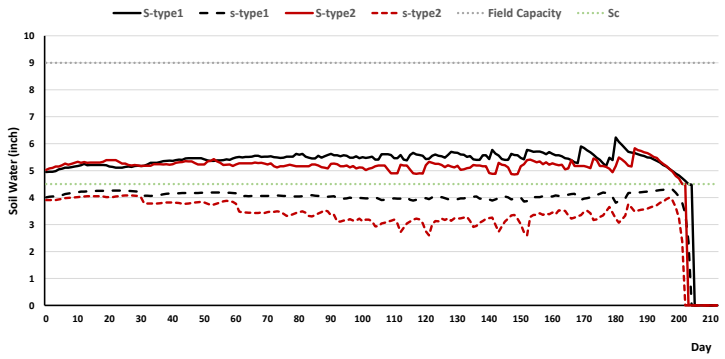

Figure 10: (s, S) values for type 1 and type 2 policies for alfalfa.

mance metrics show that compared to the FC policy, proposed (s, S) policies generate comparable net returns (0.8% and -0.54% change for type 1 and 2), while using significantly less water (water savings up to 17.61%). We also observe that yield decreases 3.4% and 8.4% with type 1 and 2 policies, respectively. Given the improvements especially in water savings, the proposed irrigation policy can be a good candidate for adoption by those farmers who have concerns on both profit margins and sustainability.

Table 5: Performance metrics of irrigation policies for alfalfa: 122 meter case

Metric (per acre)	(S,s)-Type1	(S,s)-Type2	FC	2 inch
Net Return	4.84	4.77	4.79	4.71
Yield	8.6	8.15	8.9	8.9
Water used	35.47	31.87	38.68	39.52

Table 6: Improvement when replaced with (S,s)-Type1 and (S,s)-Type2 policies: 122 meter case. (The ordered pair (a%, b%) is the change with type 1 and 2 policies, respectively.)

Metric	FC	2 inch
Net return improvement	(0.8%, -0.54%)	(2.7%, 1.34%)
Yield change	(-3.4%, -8.4%)	(-3.4%, -8.4%)
Water savings	(8.32%, 17.61%)	(10.26%, 19.36%)

In addition, we conduct a sensitivity analysis on the well depth. As discussed above, following extended droughts and increasing water usage, well depths have been increasing in the recent years. Irrigation cost is a function of several parameters including the depth of the water source. Thus, we repeat our analysis above (assuming a median of 122-meter well depth) for 92 and 161 meters that are the 25th and 75th percentiles, respectively, in our dataset. Following Eisenhauer et al. (2021), we calculate the variable irrigation costs to be \$18.57 and \$29.04 per inch per acre and fixed

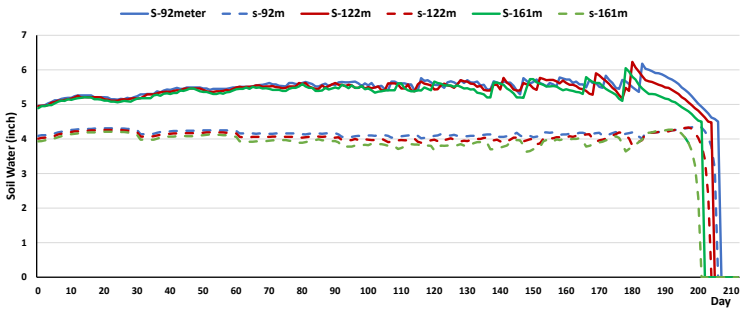

Figure 11: (s, S) values for type 1 policy for various well depths for alfalfa.

irrigation costs to be \$3.71 and \$5.81 per acre for 92-meter and 161-meter cases, respectively.

Figure 11 presents the (S, s) values of type 1 policy for the 92, 122, and 161 meter cases. This figure reveals that as the depth of the well increases, both the s and S threshold trajectories shift down. This is a result of the increasing irrigation cost with the well depth. We also observe the same pattern for the type 2 policy.

Furthermore, we repeat the analysis presented in Tables 5 and 6 for the 92 and 161 meter cases. Tables 7 and 8 compare the irrigation policies for the 92-meter case. Compared to the FC policy, we observe that proposed type 1 and 2 (s, S) policies use significantly less water (water savings up to 10.29%) at the expense of a slight decrease in net return (-0.25% and -1.38% decrease for type 1 and 2). We also observe that yield decreases 2.31% and 4.67% with type 1 and 2 policies, respectively. Compared to 2 inch policy, we observe even higher water savings (up to 12.19%) without compromising any net return (1.03% and -0.11% change for type 1 and 2). In this case, yield also ecreases 2.31% and 4.67% with type 1 and 2 policies, respectively.

Tables 9 and 10 compare the irrigation policies for the 161-meter case. Compared to the FC policy, type 1 and 2 (s, S) policies significantly improve the net return (up to 3.45%) and achieve substantial water savings (up to 29.64%). We observe that total yield decreases 5.05% and 15.37% with type 1 and 2 policies, respectively. Compared to 2 inch policy, we observe even higher net

Table 7: Performance metrics of irrigation policies for alfalfa: 92 meter case

Metric (per acre)	(S,s)-Type1	(S,s)-Type2	FC	2 inch
Net Return	5.6	5.53	5.61	5.54
Yield	8.69	8.48	8.9	8.9
Water used	36.43	34.7	38.68	39.52

Table 8: Improvement when replaced with (S,s)-Type1 and (S,s)-Type2 policies: 92 meter case. (The ordered pair (a%, b%) is the change with type 1 and 2 policies, respectively.)

Metric	FC	2 inch
Net return improvement	(-0.25%, -1.38%)	(1.03%, -0.11%)
Yield change	(-2.31%, -4.67%)	(-2.31%, -4.67%)
Water savings	(5.83%, 10.29%)	(7.82%, 12.19%)

return and water savings (up to 6.44% and 31.13%, respectively).

Our numerical analysis confirms that, similar to the corn case presented in Section 3.1.2, the proposed (s, S) type irrigation policies offer substantial economic and environmental benefits to the farmers for alfalfa compared to the irrigation policies implemented in practice especially when water is scarce. That is, our extension provide robustness check showing our approach offers significant value for different crop and locations characteristics. These benefits increase significantly with the drying wells and increasing well depths, as many farmers experiencing in California currently, following the extended droughts and increasing irrigation, domestic, and public demand for freshwater in the recent years as discussed above.

Table 9: Performance metrics of irrigation policies for alfalfa: 161 meter case

Metric (per acre)	(S,s)-Type1	(S,s)-Type2	FC	2 inch
Net Return	4	3.99	3.87	3.76
Yield	8.45	7.53	8.9	8.9
Water used	34.2	27.21	38.68	39.52

Table 10: Improvement when replaced with (S,s)-Type1 and (S,s)-Type2 policies: 161 meter case. (The ordered pair (a%, b%) is the change with type 1 and 2 policies, respectively.)

Metric	FC	2 inch
Net return improvement	(3.45%, 3.18%)	(6.44%, 6.16%)
Yield change	(-5.05%, -15.37%)	(-5.05%, -15.37%)
Water savings	(11.6%, 29.64%)	(13.47%, 31.13%)

In addition, we also study the case where the alfalfa field is composed of heterogeneous soil types. To do so, as in Section 4.1, we study the heterogeneous field example presented in Figure 4(a). This field is composed of silt loam, silty clay, and loamy sand soil types. For these soil types, normalized field capacities are 9, 12, and 5.5 inches, respectively, at the 5 feet of effective root depth we assumed for alfalfa. The field is divided into 8 IMZs as depicted in Figure 4(b). In practice, farmers manage the irrigation of each IMZ based on the soil type with the lowest available water

Table 11: Performance metrics of irrigation policies on heterogonous field for alfalfa.

Metric (field average per acre)	Heuristic	FC	2-inch
Net Return	4.99	4.73	4.68
Yield	8.66	8.9	8.9
Water used	34.65	39.29	39.84

Table 12: Improvement when replaced with the proposed heuristic policy on heterogonous field for alfalfa.

Metric (field average per acre)	FC	2-inch
Net return improvement	5.31%	6.63%
Yield change	-2.7%	-2.7%
Water savings	11.82%	13.04%

capacity as discussed in Section 4.1 in detail.

Table 11 compares the heuristic irrigation policy we propose in Section 4 ($(s, S) - LB_i$ or $(s, S) - UB_i$, for $i = 1, 2$) with the heterogonous field versions of FC and 2-inch irrigation policies employed in practice. This comparison assumes the well depth of 122 meters, which is the median depth in our well completion reports dataset discussed above. To select the heuristic policy, we implement $(s, S) - LB_i$ and $(s, S) - UB_i$, for $i = 1, 2$, policies in a simulation model representing the example field in Figure 4. For each IMZ, we compare them in terms of net return and selected the best one as the heuristic policy, which incidently corresponds to a policy based on tracking soil type with the lowest available water capacity (similar to the practice employed by farmers). Tables 11 and 12 compare the irrigation policies in terms of normalized net return (normalized revenue minus irrigation cost), yield, and water usage. All metrics are provided for the field average per acre of land. These performance metrics reveal that proposed heuristic policy can generate higher net returns (up to 6.63%), while using significantly less water (water savings up to 13.04%). We also observe that the heuristic policy can reduce the yield by 2.7% in our example field. Given the improvements in both net return and water savings, the proposed heuristic irrigation policy can also be a good candidate to be implemented also on heterogenous fields by those farmers who have concerns on profit margins and sustainability as in the homogeneous case.

C Climate Dataset Summary

In section 3.1, we present numerical study based on corn growing at Brule, NE. For this analysis, we use climate data from Nebraska Mesonet Keystone weather station that is located nearby Brule, NE. This dataset includes daily PET and precipitation measurements between 1997 and 2018. For each growing stage, we fit a discrete probability distribution to the daily PET values. Similarly, using our dataset, we compute daily rain probability and average rainfall amount (inches) per rainy day and per month during the growing season. Figure 12(a) presents average daily PET as a function of time during the corn growing season. Figure 12(b) presents daily rain probability and average rainfall amount (inches) per rainy day and per month during the corn growing season. Figures 13 and 14 present daily PET and rainfall histograms for various corn growing stages and months, respectively.

In addition, Appendix B presents a supplementary numerical study for alfalfa production in Parlier, California. For this analysis, we use climate data from CIMIS Parlier weather station. This dataset includes daily PET and precipitation measurements between 2000 and 2022. Figures 15 and 16 present daily PET and rainfall (per rainy day) histograms for a sample of months.

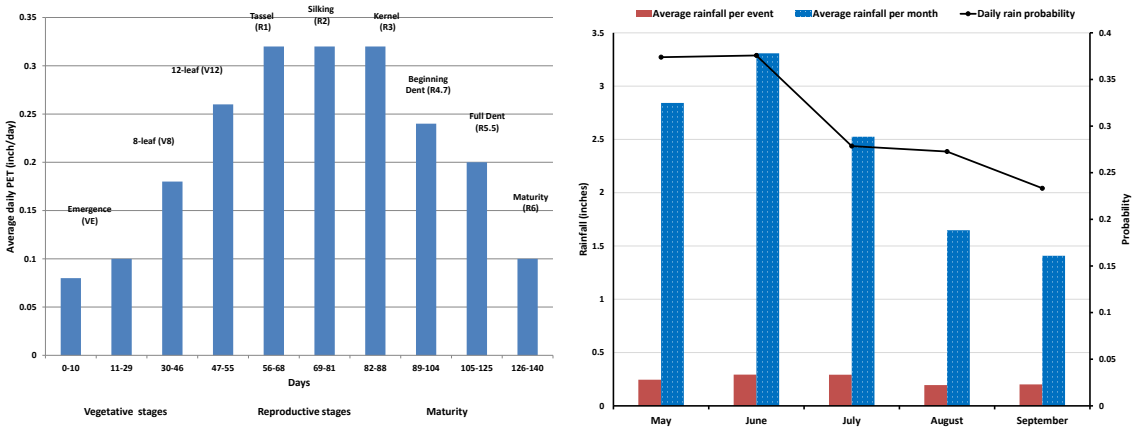

(a) Average daily PET (inch/day). (b) Rainfall.

Figure 12: PET and rainfall patterns.

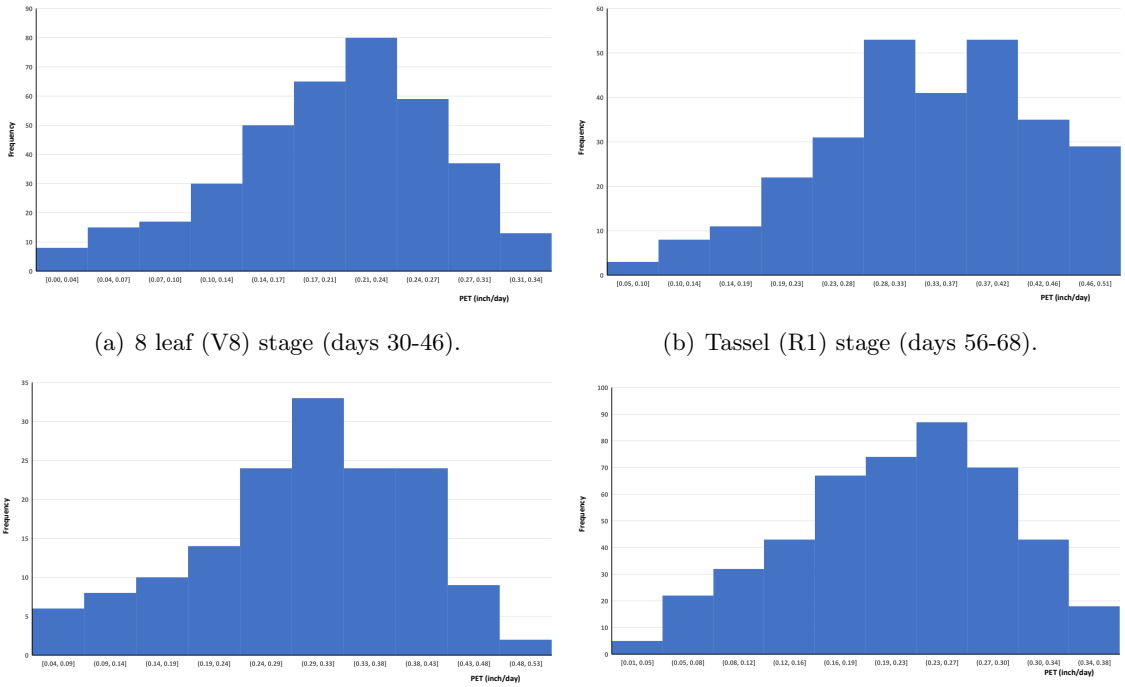

(a) 8 leaf (V8) stage (days 30-46).

(b) Tassel (R1) stage (days 56-68).

(c) Kernel (R3) stage (days 82-88).

(d) Full Dent (R5.5) stage (days 105-125).

Figure 13: Histograms of daily PET values at Keystone, NE station.

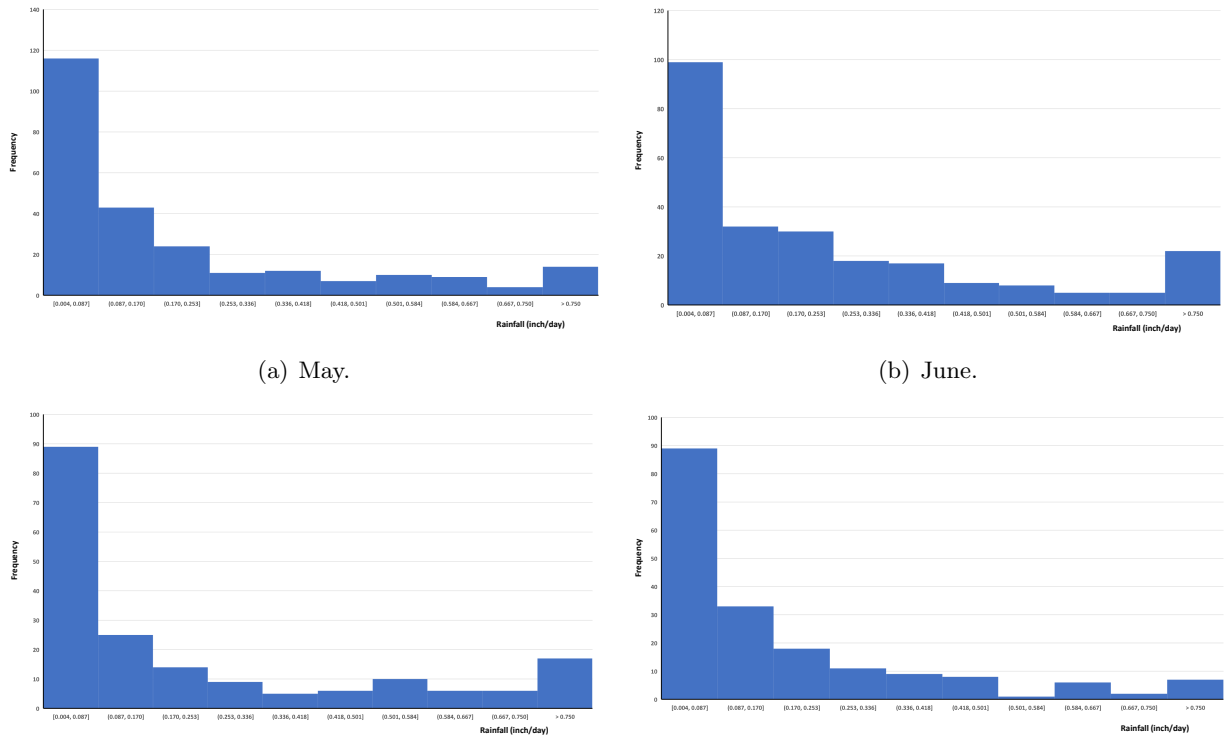

(a) May.

(b) June.

(c) July.

(d) August.

Figure 14: Histograms of daily rainfall at Keystone, NE station.

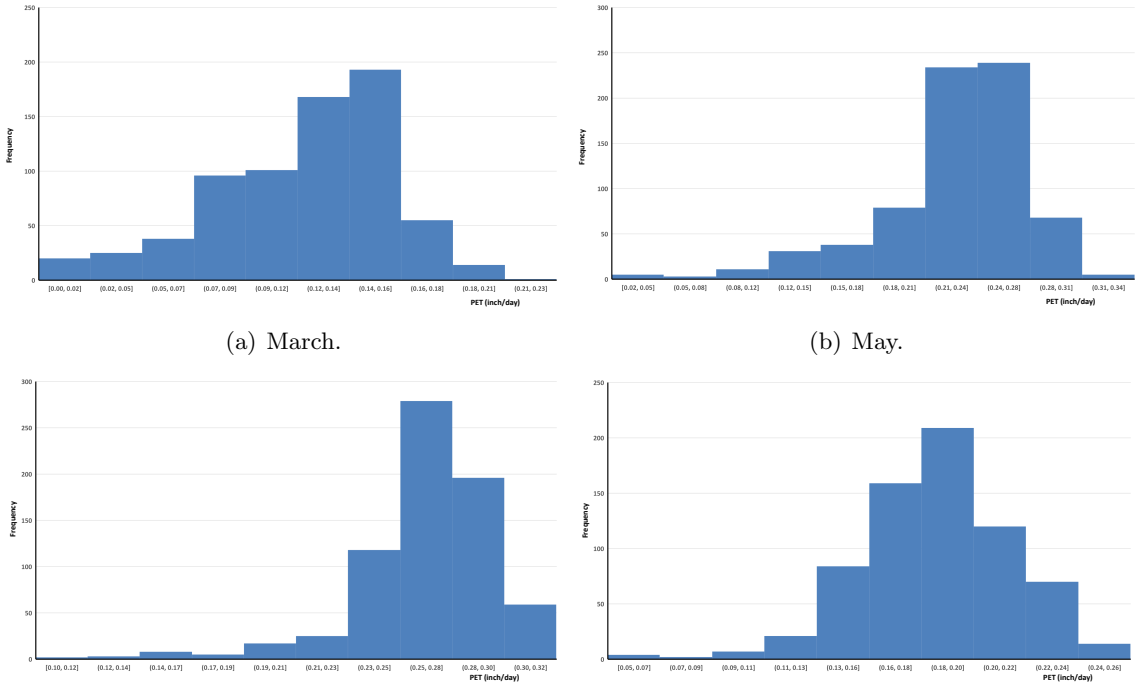

(a) March. (b) May.

(c) July. (d) September.

Figure 15: Histograms of daily PET values at Parlier, CA station.

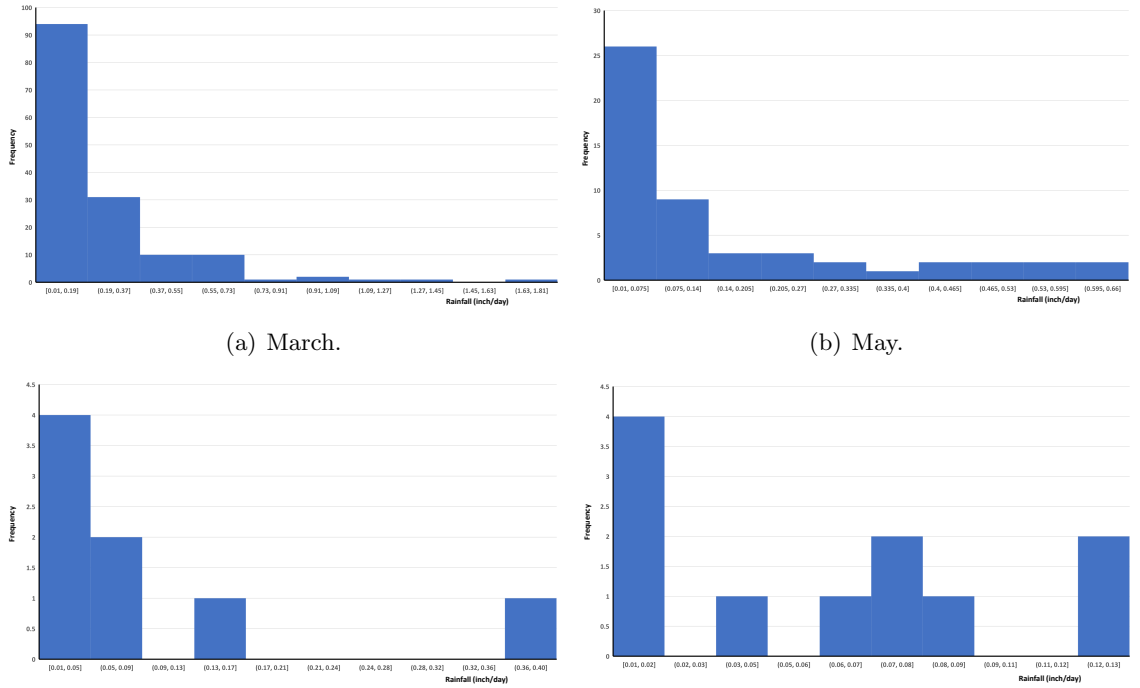

(a) March. (b) May.

(c) July. (d) September.

Figure 16: Histograms of daily rainfall at Parlier, CA station.

D Summary of Numerical Study Parameters

In our formulation, soil water content indicates the amount of water present in the soil. It is commonly expressed as the amount of water (for instance in mm of water depth) present in a given depth of soil (for instance in one meter depth of soil) at a unit area of soil. When $150mm$ of water is present in a depth of one meter of soil, the soil moisture content is $150mm/m$ (see Figure 17 below).

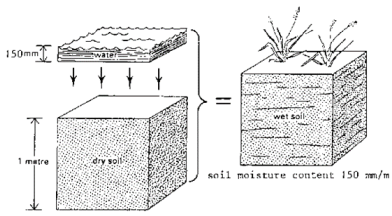

Figure 17: Soil water content. (Source: http://www.fao.org/docrep/r4082e/r4082e03.htm).

The soil water content can also be expressed in percent of volume. In the example above, $1m^3$ of soil (e.g. with a depth of $1m$, and a surface area of $1m^2$) contains $0.150m^3$ of water (e.g. with a depth of $150mm = 0.150m$ and a surface area of $1m^2$). This results in a soil water content in volume percent of 15%. Thus, a soil water content of $150mm/m$ corresponds to a water content of 15 volume percent.

As we discuss in Section 3, crop yield is strongly correlated with the amount of water stored in the soil around the crop's root zone. Thus, soil water content (along with field capacity and wilting point) is defined for the depth of crop's effective root zone. In our numerical study presented in Section 3.1, we assume that the effective root zone for corn is 4 feet, following Irmak and Rudnick (2014), and define all our soil parameters for a depth of 4 feet soil. Thus, soil water content is the depth of water in 4 feet depth of soil per unit soil area. Likewise, both the irrigation and rainfall are also measured as the depth of water (in mm or inches) per unit soil area. One could also use the volumetric measurement for all parameters (as in Irmak (2015)) instead of the depth of water. Both measurement units are used in practice and in the agriculture literature.

Furthermore, soil parameters depend on the soil type and can vary spatially across a given field. Figure 18 presents field capacity and wilting point for various soil types and Figure 19 presents an example of spatial soil variability at a field located in Saunders County, Nebraska.

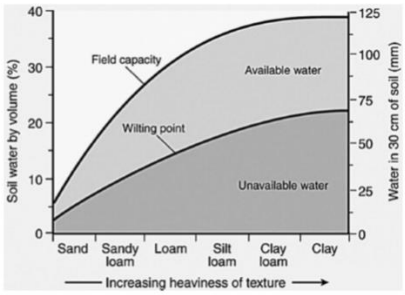

Figure 18: Soil texture and parameters (Source: Kaufmann and Cleveland (2008)).

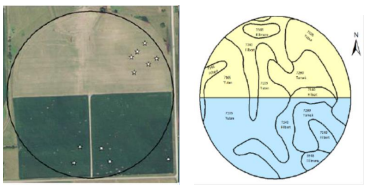

(a) Field A in Saunders, Nebraska.

(b) Boundaries of various soil types on field A.

Figure 19: Spatial variability of soil types on a given field (Source: Miller (2015)).

Finally, Figure 20 presents the water sensitivity index, λ_t, values, Table 13 lists notation, description, and value of the parameters used in the numerical study in Section 3.1, and Figure 21 presents the timeline of the events.

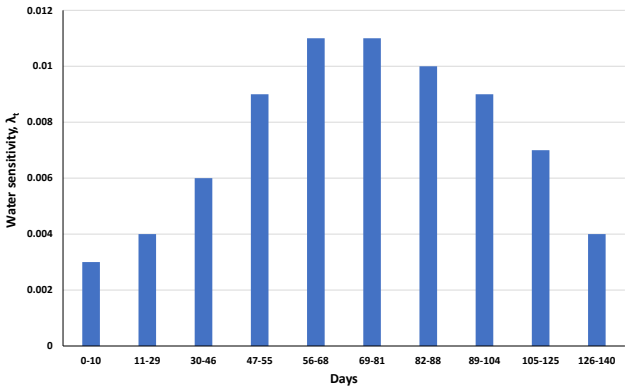

Figure 20: Daily yield water sensitivity index of corn, λ_t.

Table 13: Parameters of corn numerical study in Section 3.1

t	time index representing a day during growing season between May 10 and September 27, $t = 0, \ldots, 140$.
P_t	random variable representing daily potential ET. See Figure 12(a) for average values.
$\bar{P}_t$	average daily potential ET. See Figure 12(a) for values.
R_t	random variable representing rainfall on day t. See Figure 12(b) for average values.
λ_t	yield water sensitivity index on day t, see Figure 20 for values.
B	normalized field capacity (upper limit) for silt loam at 4 feet depth, 7.2 inches.
w	normalized wilting point (lower limit) for silt loam at 4 feet depth, 0 inches.
S^c	normalized stress threshold for silt loam at 4 feet depth, 3.6 inches.
Y_{max}	maximum attainable cumulative yield. For corn, it is 200 bushels per acre.
c	normalized variable irrigation cost, \$2.32 per inch per acre. (normalized with unit crop price)
K_f	normalized fixed irrigation cost, \$0.46 per acre. (normalized with unit crop price)

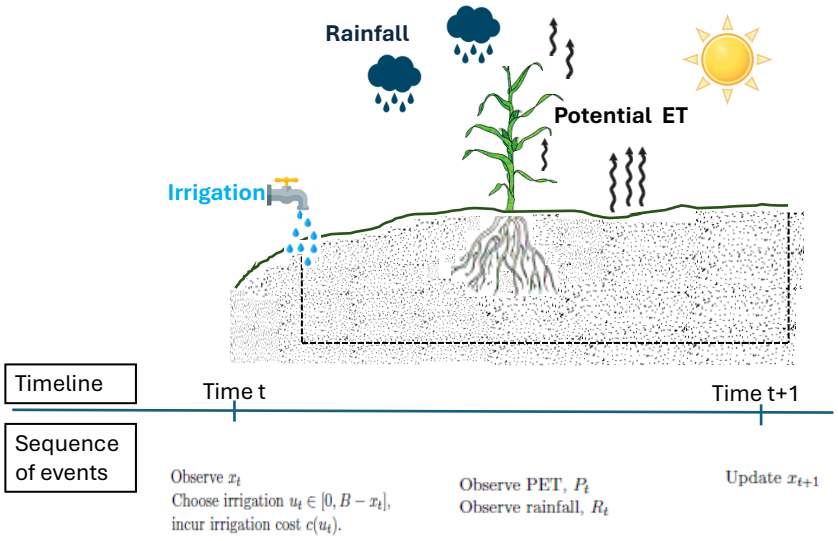

Figure 21: Timeline of events

E Sensitivity Analysis: Well-depth

In section 3.1, we conduct sensitivity analysis on well depth. Figure 22 presents the (s, S) values of our type 1 policy for the 0, 60, and 120 meter cases. This figure reveals that as the depth of the water source increases, both the s and S threshold trajectories shift down. This is a result of the increasing irrigation cost with the depth of the water source. We also observe the same pattern for the type 2 policy. In addition, Tables 14 and 15 repeat the comparison of irrigation policies for the 120-meter well depth scenario.

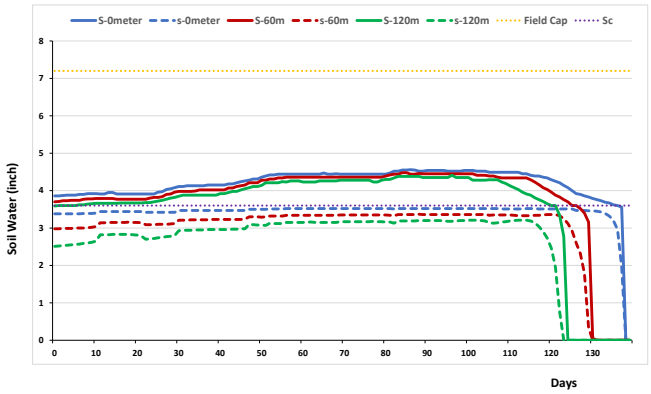

Figure 22: (s, S) thresholds of type 1 policy for various well depths.

Table 14: Performance metrics of irrigation policies on a homogeneous field: 120-meter case

Metric (per acre)	(S,s)-Type1	(S,s)-Type2	25mm	35mm	FC
Net Return	126.55	125.6	117.75	120.76	121.07
Yield	190.28	179.24	200	200	200
Water used	16.61	13.98	21.45	20.66	20.56

Table 15: Improvement when replaced with (S,s)-Type1 and (S,s)-Type2 policies: 120-meter case. (The ordered pair (a%, b%) is the change with type 1 and 2 policies, respectively.

Metric	25mm	35mm	FC
Net return improvement	(7.47%, 6.66%)	(4.79%, 4%)	(4.52%, 3.74%)
Yield change	(-4.86%, -10.38%)	(-4.86%, -10.38%)	(-4.86%, -10.38%)
Water savings	(22.54%, 34.82%)	(19.56%, 32.31%)	(19.18%, 32%)

F Optimization of Policy Parameters

Stress-avoidance policies used in practice (discussed in Section 3.1.2) target yield maximization by avoiding crop's water stress. To do so, each time soil water level decreases to the stress threshold S^c, a constant amount of water is applied. Restricting our attention to such policies, we consider the objective of maximizing net return in this appendix. That is, we study the best constant irrigation amount for a stress-avoidance policy to maximize the net return.

Following our notation in Section 3, let u denote the fixed irrigation amount to be used each time the water level decreases to S^c. We define random variable $n(u)$ representing the number of irrigation events throughout the growing season when irrigation amount is u. Let $Y(u)$ be the total yield at the end of the season. Note that since stress avoidance policies never allow for water stress, $Y(u) = Y_{max}, \forall u$. Parameters c and K_f are the normalized variable (per inch of water) and fixed irrigation costs (normalized with respect to crop price). In Section 3.1, we assumed that fixed cost is associated with the 0.2 inches of water lost at every irrigation event, thus, $K_f = 0.2 * c$. We then formulate objective function for maximizing normalized net return (yield - irrigation cost) as follows:

$$\max_u Y_{max} - (c \cdot u \cdot n(u) + 0.2 \cdot c \cdot n(u)) = \min_u c \cdot u \cdot n(u) + 0.2 \cdot c \cdot n(u) \tag{40}$$

$$= \min_u n(u)(u + 0.2). \tag{41}$$

Equations 40 and 41 show that for stress-avoidance policies, maximizing net return corresponds to minimizing total irrigation water used. This is because all such policies achieve the maximum yield, Y_{max}, and the irrigation cost scales with unit variable cost, c (since fixed irrigation cost, K_f, is proportional to c). Thus, we follow the same optimal u across different cost (well-depth) scenarios.

Figure 23 presents net return as a function of fixed irrigation amount, u, for different well depths. We observe that 2.6 inches is the optimal quantity for all cases. In addition, net return is flat for quantities beyond 1-inch.

Furthermore, we also study the sensitivity of our (s, S) policies' performance to the slope of the linear actual ET approximation, s_i (see Equation 5). Figure 24 presents the net return as a

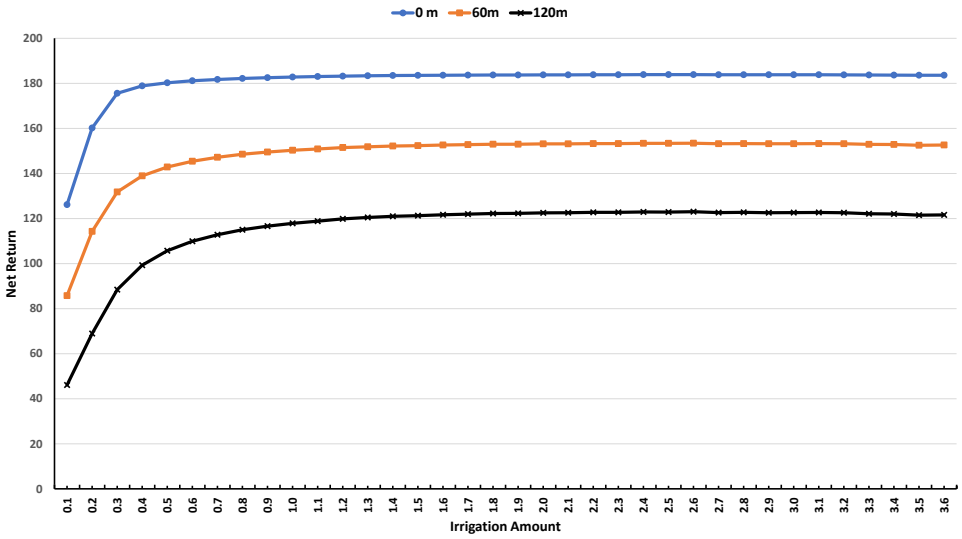

Figure 23: Net return under different fixed irrigation amounts.

function of the approximation slope for 60 meter well depth. We observe that the net return is robust to the slope value used for the AET approximation around the slope corresponding to the highest net return.

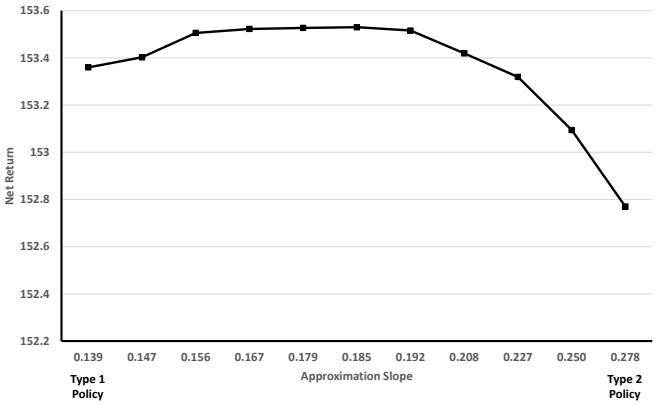

Figure 24: (S, s) policy net return under different approximation slopes for 60 meters case.

G Impact of Precision Irrigation Control Option

There are three precision control options for spatially varying irrigation rates - uniform (i.e., no variable rate capability), speed control, and zone control - as discussed in Section 4. Any irrigation policy can be implemented under any of these control settings. For instance, the FC policy can be paired with uniform control in the heterogeneous field shown in Figure 4(a), where the entire field receives the same irrigation depth based on soil moisture tracking in the lowest capacity soil type (loamy sand). Under this configuration, the field effectively consists of a single IMZ (Figure 25(a)). Alternatively, the FC policy can be implemented with speed control across IMZs, as described in Section 4.1, in which case the field is partitioned into eight IMZs that are managed independently (Figure 25(b)). Finally, the FC policy may also be combined with zone control, which enables independent regulation of sprinkler groups along the pivot arm and thereby allows finer IMZ delineation by subdividing the pivot laterally. Under this option, the field can be divided into three IMZs (each corresponding to a uniform soil type), permitting independent management of each soil type (Figure 25(c)).

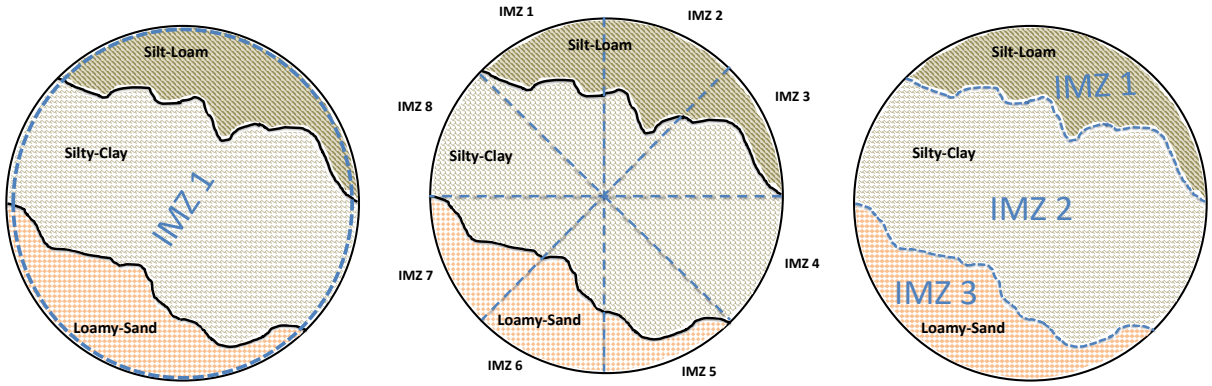

(a) Uniform. (b) Speed Control. (c) Zone Control.

Figure 25: IMZs created under different precision control options

We evaluate the policies under these three precision control levels and analyze the impact of both policy and precision technology on efficiency (net return) and sustainability (water savings). Figure 26 reports the efficiency and sustainability improvements for the FC and the proposed (s, S) policy under different control options for the heterogeneous field in Figure 4. In the figure, both vertical axes show percentage improvements relative to an FC policy with uniform irrigation, and

the precision level increases from left to right - from uniform to speed to zone control.

Figure 26 demonstrates that both the irrigation policy and the precision control technology contribute to efficiency and sustainability gains. Farmers can attain substantial net-return improvements and water savings by adopting more efficient irrigation policies (such as the proposed (s, S) policy) even without precision agriculture technologies. These policies can further amplify the benefits of existing precision control tools (e.g., speed and zone control). We observe similar patterns when comparing against other policies commonly used in practice, such as the 25mm and 35mm rules discussed in sections 3.1 and 4.1.

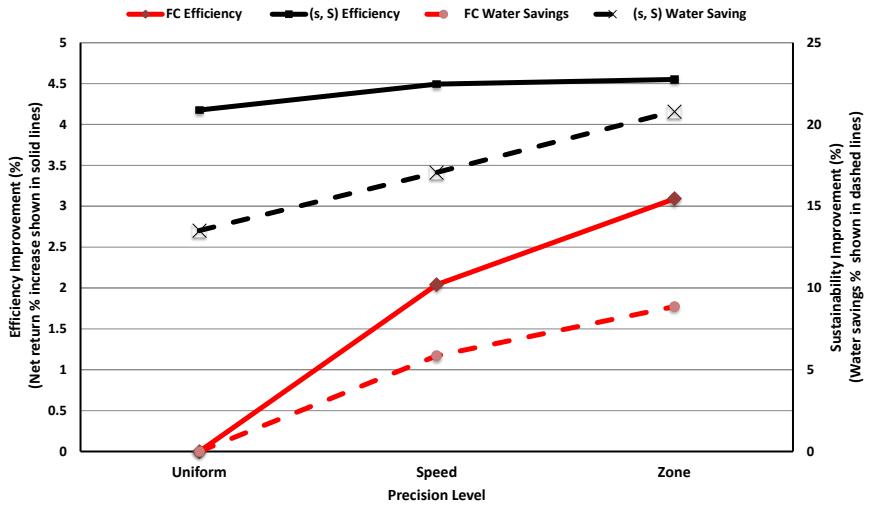

Figure 26: Efficiency and sustainability improvements under various precision control options.

References

Hansen, B. R., K. H. Bali, and L. S. Blake (2008). Irrigating alfalfa in arid regions. Chapter 7. In C. G. Summers, and D. H. Putnam (Eds.), Irrigated alfalfa management for Mediterranean and desert zones. Oakland: University of California Agriculture and Natural Resources Publication, 8293, See: http://alfalfa.ucdavis.edu/IrrigatedAlfalfa.

Kaufmann, R. K., and C. J. Cleveland (2008). *Environmental Science*. (1st edition). McGraw-Hill.

Putnam, D. H., C. G. Summers, and S. B. Orloff (2007). Alfalfa production systems in California. Chapter 1. In C. G. Summers, and D. H. Putnam (Eds.), Irrigated alfalfa management for Mediterranean and desert zones. Oakland: University of California Agriculture and Natural Resources Publication, 8287, See: http://alfalfa.ucdavis.edu/IrrigatedAlfalfa.

Steduto, P., T. C. Hsiao, E. Fereres, and D. Raes (2012). Crop yield response to water. FAO Irrigation and Drainage Paper No. 66, United Nations FAO, Rome, Italy.

USDA (2019). 2017 Census of agriculture. 2018 irrigation and water management survey. USDA-NASS. U.S. Department of Agriculture, National Agricultural Statistics Service.

Stokstad, E. (2020). Droughts highlighted California's unsustainable use of groundwater. Now, the state is trying to refill its aquifers. Science (April 16), https://www.science.org/content/article/droughts-exposed-california-s-thirst-groundwater-now-state-hopes-refill-its-aquifers.